



Integration of Functionalized Graphene Nano-Network into Planar Perovskite Absorber for High Efficiency Large Area Solar Cells

Journal:	<i>Materials Horizons</i>
Manuscript ID	MH-COM-05-2018-000511.R1
Article Type:	Communication
Date Submitted by the Author:	14-Jun-2018
Complete List of Authors:	<p>Wang, Yong; Shanghai Jiao Tong University Zhou, Yuanyuan; Brown University, School of Engineering Zhang, Taiyang; Shanghai Institute of Technology, Ju, Minggang; University of Nebraska-Lincoln, Department of Chemistry Zhang, Lin; Brown University, School of Engineering Kan, Miao; Shanghai Jiao Tong Univeristy, School of Environmental Science and Engineering Li, Yihui; Shanghai Jiao Tong University Zeng, Xiao; University of Nebraska-Lincoln, Chemistry Padture, Nitin; Brown University, School of Engineering Zhao, Yixin; Shanghai Jiao Tong Univeristy, School of Environmental Science and Engineering</p>

Conceptual Insights for the manuscript

Integration of Functionalized Graphene Nano-Network into Planar Perovskite Absorber for High Efficiency Large Area Solar Cells

Yong Wang, Yuanyuan Zhou, Taiyang Zhang, Ming-Gang Ju, Lin Zhang, Miao Kan, Yihui Li, Xiao Cheng Zeng, Nitin. P. Padture, Yixin Zhao^{a*}

The high charge collection efficiency in lead halide perovskite solar cells are most critical to their high efficiency in commercialization of this promising low-cost and high-efficiency photovoltaic technology. In the (quasi)-planar configuration perovskite solar cells, the charge collection carried out on the 2D interface to 2D interface between perovskite absorber top surface layer and planar charge collection layer. The tremendous grain boundary 3D-likely distributed in these polycrystalline perovskite absorber layer could hinder the charge collection efficiency. In this study, we demonstrated a quasi-3D charge collection nano-network configuration for the design of large-area planar perovskite solar cells with enhanced the collection efficiency. The integration of an unprecedented functionalized graphene nano-network into perovskite absorber layer leads to a form a quasi 3D charge collection combined with typical 2D charge-collection layer. This quasi 3D charge collection configuration significantly enhances $1 \times 1 \text{ cm}^2$ MAPbI₃ PSCs' power conversion efficiencies from 14.4 to 18.7% with higher reproducibility, less hysteresis and enhanced stability. The

concept to introducing a quasi-3D charge collection configuration into perovskite absorber layer would be a promising strategy to pave the way for high-performance and large area perovskite solar cell devices.



Journal Name

COMMUNICATION

Integration of Functionalized Graphene Nano-Network into Planar Perovskite Absorber for High-Efficiency Large-Area Solar Cells

Received 00th January 20xx,
Accepted 00th January 20xx

DOI: 10.1039/x0xx00000x

www.rsc.org/

Yong Wang,^a Yuanyuan Zhou,^b Taiyang Zhang,^a Ming-Gang Ju,^c Lin Zhang,^b Miao Kan,^a Yihui Li,^a Xiao Cheng Zeng,^c Nitin. P. Padture^b and Yixin Zhao^{a*}

Efficient charge collection is critical in large area (quasi-) planar configuration perovskite solar cells (PSCs) as the cell operation relies on the diffusion of photo-generated charge carriers to charge collector layers. Many defects/traps in the polycrystalline perovskite absorber layer strongly affect the charge collection efficiency because the 2D-like top charge collection layer barely penetrates into the 3D grain boundaries in perovskite layer to efficiently collect the charge carrier. Inspired by blood capillaries for efficient mass exchange, a charge-collection nano-network for efficient charge collection was incorporated into the perovskite absorber using low-cost, stable amino-functionalized graphene (G-NH₂). The integration of such an unprecedented structure enables very efficient charge collection, leading to the significant enhancement of 1×1 cm² MAPbI₃ PSCs' power conversion efficiencies from 14.4 to 18.7% with higher reproducibility, less hysteresis and enhanced stability. The physicochemical mechanisms underlying the role of this nano charge-collection nano-network in boosting the charge collection in PSCs are elucidated comprehensively, using a combined experimental and theoretical approach, pointing to a new direction towards up-scaling of high-efficiency PSCs.

Introduction

Perovskite solar cells (PSCs), with their unprecedented power conversion efficiency (PCE) progress, have enormous potential as next-generation photovoltaics (PVs) for the clean-energy future.¹⁻³ The certified record PCE of PSCs has quickly approached 23%, which is comparable to PCEs of crystalline

silicon solar cells.⁴ In general, PSCs employ solution-deposited polycrystalline organic-inorganic halide perovskite thin films as the light absorber.^{5, 6} Due to the high-density of grain boundaries (GBs), these polycrystalline perovskite thin films contain abundant defects/traps to deteriorate the charge collection efficiency.^{7, 8} Reducing defects/traps in the perovskite absorber layer, and thereby improving the charge-collection efficiency in PSCs, has become one of most popular strategy for achieving maximum PCE, which is critical for the successful commercialization of this promising low-cost, high-efficiency PV technology.⁹

The state-of-the-art high-efficiency PSCs are invariably based on (quasi-) planar device configurations, where the two charge collection layers (CCLs) sandwich the perovskite absorber layer to collect the charge carriers that are generated in the perovskite bulk and diffuse to the perovskite/CCLs interfaces.¹⁰⁻¹³ The charge collection process occurs mainly at the interface between the perovskite absorber layer and the CCLs. The carrier diffusion lengths in planar perovskite thin films are considered long, resulting in a high charge-collection efficiency in PSCs.^{14, 15} Nevertheless, there is still considerable charge-collection loss due to the defects/traps at GBs in the perovskite absorber layer.¹⁶⁻¹⁸ Such charge-collection loss can be even more severe in large-area PSC devices, which not only reduces their PCEs but also lowers the device reproducibility.^{19, 20} One straightforward strategy to increase the charge-collection efficiency is to enhance or modify the charge-collection interfaces.^{21, 22} In the literature, carbon-based materials with excellent charge transfer properties and high chemical stability have been employed as a new charge collection layer or as a modifier in the existing charge-collection layer in PSCs.²³⁻²⁵

Inspired by the effective mass exchange in the blood capillaries, we demonstrate an unprecedented strategy to boost the charge collection in PSC devices via incorporating a carbon-based charge-collection nano-network into the CH₃NH₃PbI₃ (MAPbI₃) perovskite absorber layer. The construction of the carbon-based charge collection nano-network was realized via simply adding amino-functionalized

^a School of Environmental Science and Engineering, Shanghai Jiao Tong University, 800 Dongchuan Road, Shanghai 200240, China

^b School of Engineering, Brown University, Providence, Rhode Island 02912, United States

^c Department of Chemistry, University of Nebraska-Lincoln, Lincoln, Nebraska 68588, United States

E-mail: yixin.zhao@sjtu.edu.cn

† Footnotes relating to the title and/or authors should appear here.

Electronic Supplementary Information (ESI) available: [details of any supplementary information available should be included here]. See DOI: 10.1039/x0xx00000x

graphene (G-NH₂) into the MAPbI₃ precursor solution, followed by co-precipitation of G-NH₂ and MAPbI₃ perovskite. The integration of the functionalized graphene in perovskite layer not only induces the formation of large grain size perovskite crystals but also helps the formation of the nano-network in the MAPbI₃ perovskite absorber layer. Consequently, the 1×1 cm² large area MAPbI₃ PSCs with the in-situ integrated nano-network exhibits power conversion efficiencies up to 18.7% with higher reproducibility, less hysteresis and enhanced stability than the 14.2% efficiency control ones.

Results and discussion

Figure 1a shows topographic images of as-prepared G-NH₂ taken using an atomic force microscopy (AFM). The thickness of G-NH₂ is about 0.8 nm (Figure S1), and their lateral size is submicron. Fourier transform infrared spectroscopy (FTIR) spectrum in Figure 1b confirms the amino group in these G-NH₂ samples. Also, TEM results indicate that the as-prepared G-NH₂ is composed of few-layer transparent graphene sheets with homogeneous elemental distribution of C, N on the graphene sheets (Figure S2). The G-NH₂ can be well-dispersed in the MAPbI₃ precursor solution in mixed DMF/DMSO (v/v

ratio, 4:1) solvent. As shown in Figure S3, after the addition of G-NH₂, the MAPbI₃ precursor solution appears darker. It is found that the introduction of G-NH₂ has some obvious effects on the microstructures of as-deposited MAPbI₃ perovskite thin films. Figure S3 reveals that the incorporation of G-NH₂ has a negligible effect on the UV-vis spectra of the MAPbI₃ perovskite films. The absorbance edges of both thin films are located at ~780 nm, which is consistent with previous results.²⁶ Figure 1c and 1d show that both MAPbI₃ and MAPbI₃/G-NH₂ thin films are compact, pinhole-free, and full-coverage, which is typical of thin films prepared using the solvent-engineering method.^{5,6,27} However, the MAPbI₃/G-NH₂ thin film has larger grains and smoother surface in comparison with the pure MAPbI₃ thin film. In the MAPbI₃/G-NH₂ thin film, the average grain size is >500 nm with the largest grains >1 μm, whereas the pure MAPbI₃ thin film has an average grain size of ~300 nm. The enlarged grains might be attributed to the high dispersion of G-NH₂ at MAPbI₃ grain boundary which tailors the grain boundary migration process during the thermal annealing stage.²⁸ More detailed studies will be performed in the future to elucidate this effect. The 3D AFM images in Figures S4 show that the root mean square (RMS) roughness of the MAPbI₃/G-NH₂ thin film top-surface is 6.6 nm, smaller than the 10.2 nm RMS roughness of the pure MAPbI₃ thin film.

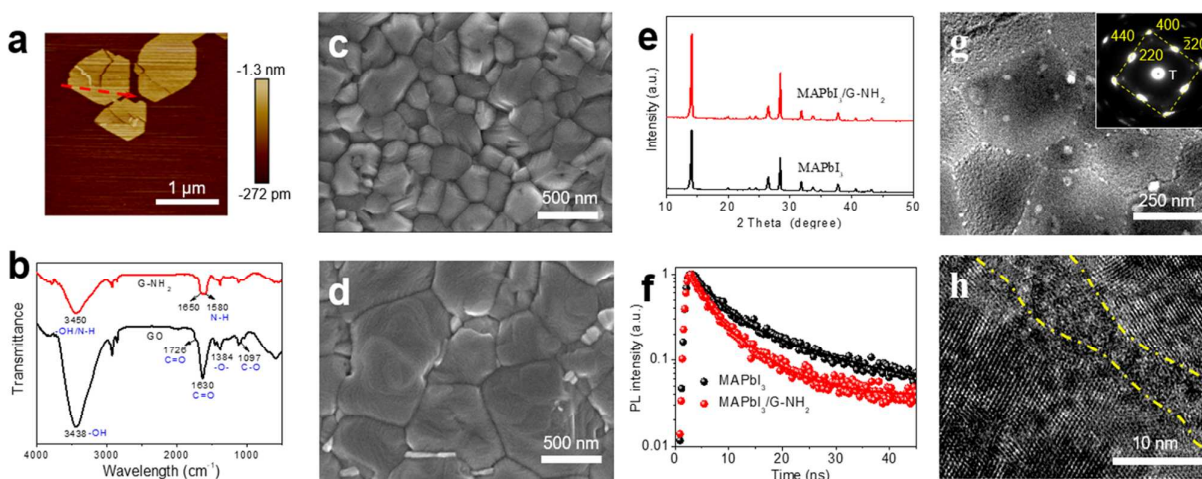


Figure 1 G-NH₂: (a) Topographic AFM image, (b) FTIR spectroscopy of G-NH₂. SEM of thin films: (c) MAPbI₃ and (d) MAPbI₃/G-NH₂. (e) XRD patterns of the MAPbI₃ thin films with and without the optimal G-NH₂ addition. (f) TRPL decay curves of MAPbI₃, and MAPbI₃/G-NH₂ thin films. The measurements were performed from the perovskite film side. (g) Bright-field TEM image of the MAPbI₃/G-NH₂ thin film, and (h) HRTEM image of the GB region (between dashed yellow lines).

The XRD patterns of both the MAPbI₃/G-NH₂ and pure MAPbI₃ perovskite thin films show strong diffraction peaks at 14.1°, 28.4° and 31.8° (Figure 1e), which are respectively assigned to 110, 220 and 310 reflections in the typical tetragonal phase of MAPbI₃ perovskite.²⁹ The intensity of XRD peaks for the MAPbI₃/G-NH₂ thin film is stronger than that for the pure MAPbI₃ perovskite, suggesting that the G-NH₂ incorporation enhances the overall crystallinity of the thin film. In addition, we have found that amount of G-NH₂ incorporated

in the MAPbI₃ thin films has only slight effects on the UV-vis absorption spectra, XRD patterns and grain size (Figure S5 and S6). These results indicate that the incorporation of G-NH₂ improves the crystallinity, enlarges the grain size, and smoothens the surface of the perovskite absorber film. This can be attributed to the relatively controlled nucleation and growth behavior induced by G-NH₂ as heterogeneous nucleation sites in the crystallization process.

Normally, the enhanced crystallinity and larger grain size are expected to reduce defects/traps and then increase the photoluminescence (PL) lifetimes in perovskite thin films.³⁰ However, the time-resolved PL (TRPL) responses from MAPbI₃ and MAPbI₃/G-NH₂ thin films in Figure 1f reveal that MAPbI₃ thin film's lifetime (τ_{av} =10.99 ns) is almost twice longer than MAPbI₃/G-NH₂ (τ_{av} =5.05 ns). Such abnormal decrease of PL lifetime is actually similar to the case of perovskite films covered with charge transport (carrier-quencher) layers.³¹⁻³³ The TRPL results combined with the material-characterization results in Figure 1 indicate efficient charge extraction and interface contact between G-NH₂ and MAPbI₃ perovskite crystals. Furthermore, we have also investigated the effect of reduced graphene oxide (rGO) on the MAPbI₃ perovskite film for comparison (Figure S7). Similar to G-NH₂, rGO incorporation shows a similar effect of enhanced crystallinity and enlarged grain size. However, the τ_{av} =69.23 ns for MAPbI₃/rGO thin film is much longer than that for pure MAPbI₃ (Figure S7), suggesting poor charge extraction by rGO.

In order to confirm the detailed microstructure, transmission-electron-microscope (TEM) characterization of the MAPbI₃/G-NH₂ thin film was performed. The TEM specimens were prepared using a methodology that has been successfully demonstrated for characterizing halide perovskite materials in previous reports.^{29, 34} This entails direct solution-deposition of the MAPbI₃/G-NH₂ thin film onto the TEM grid. Figure 1g is a bright-field TEM image of the MAPbI₃/G-NH₂ thin film. The perovskite grains and GBs areas are immediately differentiated from the contrast, and are labelled in Figure 1g. The typical selected-area electron diffraction pattern (SAEDP) of an individual grain is shown in the inset image in Figure 1g, which confirms the single-crystalline nature of the grains. The indexed SAEDP is consistent with the tetragonal phase of MAPbI₃ perovskite.²⁹ High-resolution TEM images of the typical GB regions were also obtained, and the result is shown in Figure 1h. It can be seen that the GB region appears relatively amorphous, which is clearly distinct from the high-crystalline state of the MAPbI₃ perovskite grain. It appears that the GB regions are decorated with the carbonaceous material (G-NH₂), which is consistent with the AFM results.

These results taken together indicate that the G-NH₂ layer buried in the perovskite absorber layer forms a G-NH₂ nano-network, which is potential to facilitate charge extraction and transport in planar PSCs. Here is another important thing we have to note that: the PSCs devices integrated with G-NH₂ nano-network show much less shorting than the control ones. This fact also suggests the G-NH₂ layer is highly likely to be buried in the perovskite absorber layer. Further, a typical planar device configuration of FTO/c-TiO₂/SnO₂/perovskite/Spiro-OMeTAD/Ag (Figure S8) is adopted for both MAPbI₃/G-NH₂- and MAPbI₃-based PSCs. MAPbI₃/G-NH₂ based devices for a size of 0.1 cm² area with different G-NH₂ content have been investigated firstly (Figure S9 and S10), and the optimized G-NH₂ content is found to be 0.05 mg·mL⁻¹ (Hereafter, MAPbI₃/G-NH₂ refers to thin films with optimized 0.05G-NH₂ content.). The PV performance statistics in Figure S10 show that all MAPbI₃/G-NH₂-based PSCs

exhibit higher PV performance than PSCs based on pure MAPbI₃. Moreover, the MAPbI₃/G-NH₂-based PSCs show an important advantage of both enhanced reproducibility with a narrow PCE distribution and less hysteresis in J-V curves (Figure S11). The champion of MAPbI₃/G-NH₂-based PSC exhibits enhanced PV performance over the MAPbI₃ (20.4% vs. 18.5%) (Table S1).

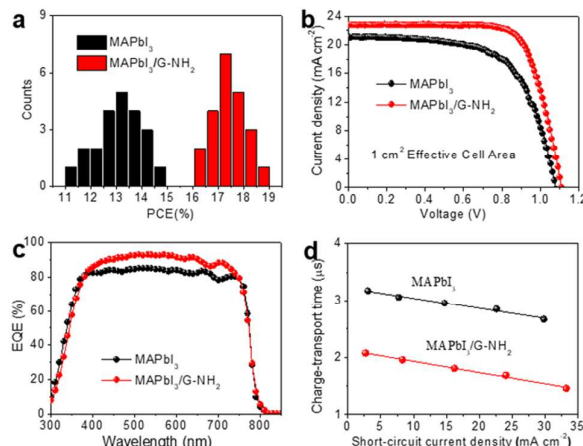


Figure 2 (a) PCE distributions of PSCs based on MAPbI₃ with and without G-NH₂ (average of 22 devices), (b) J-V characteristics for a PSCs of 1*1cm² based on MAPbI₃ with and without G-NH₂ under simulated AM 1.5G solar illumination of 100 mW·cm⁻² in reverse scan, and (c) corresponding EQE spectrum together with the integrated J_{sc} . (d) Charge transport time dependence on the J_{sc} of PSCs based on MAPbI₃ with and without G-NH₂ measured using the IMPS technique.

The application of large area PSCs devices have been bothered by the significant reduction of PCEs and the poor device reproducibility once the cell area increases. One main reason is that the large area PSCs devices are sensitive to defects/traps and charge transfer properties.^{19, 20, 35} Interestingly, the incorporation of G-NH₂ nano-network into perovskite absorber layer could significantly improve both the PCE and reproducibility of large-area devices. The PV performance parameter statistics in Figure 2a and Table S2 are obtained from the 2.5×2.5 cm² substrates with an effective cell area of 1 cm², and the MAPbI₃/G-NH₂ based PSCs are based on the optimum G-NH₂ content as the aforementioned small area ones. Excitingly, the large-area MAPbI₃/G-NH₂-based PSCs exhibit an average efficiency as high as 17.4%, while the MAPbI₃-based PSCs only have a value of 13.2%. The efficiency distribution of MAPbI₃/G-NH₂-based PSCs is narrower than the pure MAPbI₃ based PSCs, suggesting an enhanced reproducibility. Figure 2b compare the J-V curves of the champion large-area MAPbI₃/G-NH₂ and MAPbI₃ based PSCs. The MAPbI₃/G-NH₂-based device show a PCE of 18.7% with J_{sc} of 22.8 mA·cm⁻², V_{oc} of 1.11 V and FF of 0.739. In contrast, the champion large-area cell with MAPbI₃ thin film without the G-NH₂ has a PCE of only 14.4% due to the lower J_{sc} of 21.1 mA·cm⁻², lower V_{oc} of 1.08 V, and a significantly lower FF of 0.632. The large-area MAPbI₃/G-NH₂-based PSCs also exhibit

smaller hysteresis (Figure S12 and Table S3), and finally results in a stable 18.0% PCE output (Figure S13). The external quantum efficiency (EQE) of MAPbI₃/G-NH₂-based PSC in Figure 2c can be as high as 92% in the wavelength range of 500~600 nm, which is much higher than the corresponding pure MAPbI₃. Since there is no difference in the absorbance between MAPbI₃ and MAPbI₃/G-NH₂ thin films (Figure S3), the enhanced J_{SC} is attributed to the improved charge-collection efficiency in MAPbI₃/G-NH₂ with help of the charge collection nano-network. The integrated J_{SC} calculated from the EQE is 22.6 mA·cm⁻², whereas the pure MAPbI₃ device shows an intergrated J_{SC} value of 21.0 mA·cm⁻² (Figure 2c). These EQE results are consistent with the J-V measurements, and confirm the enhanced charge-collection efficiency in MAPbI₃/G-NH₂-based PSC. Moreover, the lower electronic resistance (~13 Ω) of the MAPbI₃/G-NH₂-based PSC revealed by impedance spectroscopy (EIS) characteristics under illumination in Figure S14 also confirms the better charge transfer compared to the MAPbI₃-based PSC (~33 Ω). In addition, the significant enhancement on FF in the former case could be due to the efficient charge extraction and transport by the nano-network as PSC FF is closely related to additional charge transport losses originating from inefficient charge extraction of the cells, or current leakage through shunts.³⁶

A previous report has revealed that the lower charge extraction and transport had limited the photocurrent observed in the MAPbI₃ PSCs.³⁷ Intensity modulated photocurrent spectroscopy (IMPS) measurements were

performed on the MAPbI₃- and MAPbI₃/G-NH₂-based PSCs to explore the impact of nano-network on the charge-transport properties. The charge transport in MAPbI₃/G-NH₂-based PSC is faster than that in MAPbI₃-based PSC (Figure 2d). This confirms that the incorporation of the G-NH₂ nano-network in the perovskite absorber layer facilitates charge extraction and transport for a higher charge-collection efficiency. Other than the higher charge-collection efficiency and higher performance, the MAPbI₃/G-NH₂-based PSCs exhibit better stability than PSCs based on pure MAPbI₃ perovskite in a dark box with 20-30% relative humidity (RH) and a temperature of 25-30 °C. The MAPbI₃/G-NH₂-based PSC without any encapsulation still maintains ~17% PCE after 2 months storage, whereas the PCE of the MAPbI₃-based device drops to ~8% (Figure S15).

Conducting atomic force microscopy (c-AFM) in contact mode was conducted to investigate the effect of the nano-networks on charge transport. Figure 3 shows that the average current through MAPbI₃ and MAPbI₃/G-NH₂ thin films are 198 pA and 301 pA, respectively, under 1 V direct-current (DC) bias. The current in the MAPbI₃/G-NH₂ thin film is more unevenly distributed over the surface in comparison with the pure MAPbI₃ thin film. Interestingly, the current is most prominent in the GB region (G-NH₂) in the MAPbI₃/G-NH₂ thin film as shown in Figure 3e and 3f. These results indicate that the G-NH₂ present at the GBs exhibits excellent charge transport capability.

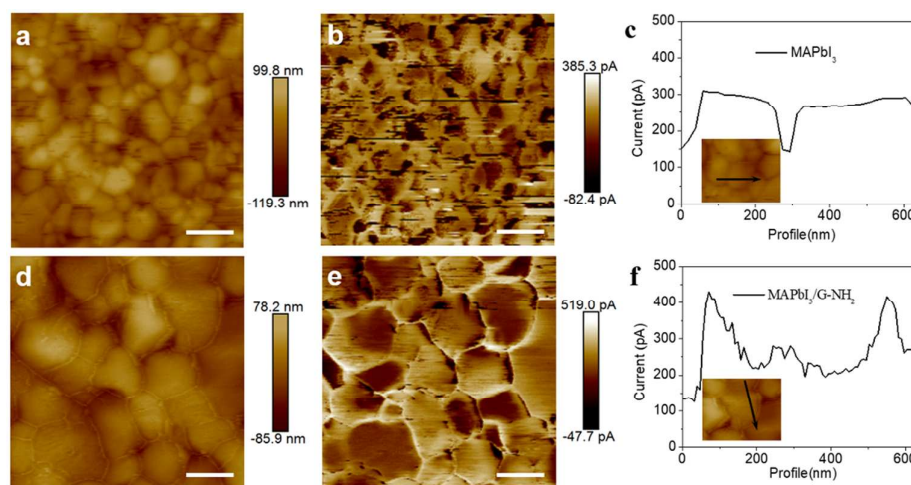


Figure 3 MAPbI₃ thin film: (a) topographic image film and (b) corresponding current image (1 V applied DC voltage), (c) c-AFM current line profiles for MAPbI₃. Inset: corresponding topographic AFM images. MAPbI₃/G-NH₂ thin film: (d) topographic image and (e) corresponding current image (1 V applied DC voltage), (f) c-AFM current line profiles for MAPbI₃/G-NH₂ thin film. Inset: corresponding topographic AFM images. Scale bars = 400 nm.

The aforementioned results suggest that the observed improvement in the J_{SC} and FF of MAPbI₃/G-NH₂-based PSCs could be attributed to the efficient charge collection by the G-NH₂-based nano-networks incorporated within the perovskite absorber layer. Usually, the defects/traps in the perovskite layer can result in recombination of charge carriers (the left

image in Figure 4a), and cause a decline in J_{SC} , V_{OC} , and, especially, FF, causing further reduction in the PCE. In fact, the defects/traps induce even more serious issues in large-area PSCs.^{38, 39} In our study, the plausible working mechanism behind this high current collection efficiency could be attributed to bypassing defect sites via the nano-network as

shown in right image in Figure 4a.

We further calculate the charge density at the interface of MAPbI₃ with G-NH₂, using the density-functional theory (DFT) method, as shown in Figure 4b. It can be seen that there is a significant charge rearrangement at the interface of G-NH₂ with MAPbI₃, forming an internal electrical field near the interface. Specifically, the negative charges gather near the G-NH₂ while the positive charges gather near the surface in the MAPbI₃ perovskite, resulting in dipoles pointing from MAPbI₃ to G-NH₂. This newly produced dipole field facilitates the hole transfer into G-NH₂ from the MAPbI₃ perovskite. For comparison, we also present the charge density at the interface of MAPbI₃ perovskite and rGO without functionalized amino group in Figure S16, where it shows a much weaker internal electrical field at the interface. This theoretical result supports the notion that the nano-network based on G-NH₂ can significantly promote charge transfer, and it also confirms that the chemisorbed amino functional group is likely responsible for these observed enhancements.

The incorporation of rGO into the MAPbI₃ perovskite absorber layer does not lead to significant improvements in PV performance (Figure S17). Furthermore, the longer PL lifetime indicates that the rGO may work mainly as a passivation layer in the MAPbI₃/rGO thin film.^{30, 40} These experimental results on rGO are consistent with the theoretical calculations (Figure S16).

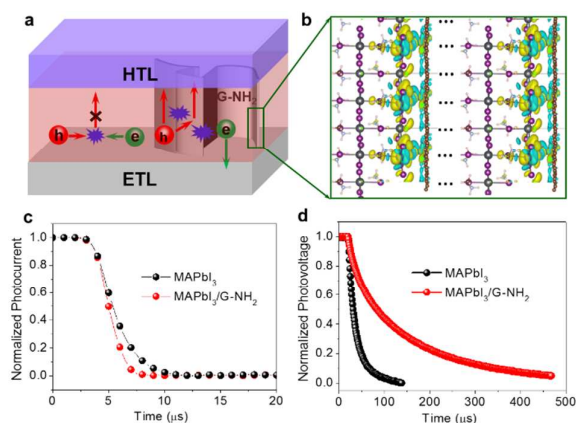


Figure 4 (a) Schematic illustrations of charge transport in PSC based on MAPbI₃ without and with G-NH₂. (b) Calculated charge density at interface between MAPbI₃ and G-NH₂ (yellow=positive, cyan=negative). Large-area (1 cm²) PSCs based on MAPbI₃ with and without G-NH₂: (c) TPC and (d) TPV.

The charge transport in the large-area devices were further investigated by transient photocurrent decay and photovoltage decay (TPC/TPV). The faster photocurrent decay response of MAPbI₃/G-NH₂-based PSC illustrates faster charge transport than in the MAPbI₃-based PSC (Figure 4c). Meanwhile, the TPV decay curve of the MAPbI₃/G-NH₂-based PSC shows a longer lifetime than in the MAPbI₃-based PSC, indicating significant decrease of charge-carrier recombination (Figure 4d). We attribute the reduced recombination to the improvement of extraction and transport of charge carriers by

the G-NH₂ nano-network. The improvements in the extraction and transport of charge-carriers in perovskite layer is beneficial for improving the J_{SC} , V_{OC} , and, especially, FF.

Conclusions

In summary, we have successfully demonstrated the construction of a charge-collection nano-network in PSCs by incorporating graphene with functionalized amino group into the MAPbI₃ perovskite absorber layer. This nano-network induces dramatically higher charge-extraction efficiency, facilitates charge transport, and finally leads to significantly enhanced PCE of large area PSCs. Planar large-area (1 cm²) PSCs incorporating this nano-network have PCEs close to 19%, with excellent reproducibility. The approach and strategy of incorporating the charge-collection nano-network could be applied to other perovskite compositions, and even to other types of solar cells, and it represents a promising new concept for achieving high-performance PVs of the future.

Author contributions

Y. Zhao conceived the idea, directed and supervised the project. Y. W. fabricated devices. Y.W., Y. Zhou, T. Z., M. J., L. Z., M. K., Y. L., X. Z. were involved in experimental and theoretical data analysis. All authors contributed to the discussions. Y. Zhao, Y. W., Y. Zhou, and N.P.P co-wrote the manuscript.

Conflicts of interest

There are no conflicts to declare.

Acknowledgment

Y. Zhao acknowledges the support of the NSFC (Grant 21777096) and Huoyingdong Grant (151046). The work performed at Brown University and UNL was supported by the U.S. National Science Foundation (NO. OIA-1538893).

References

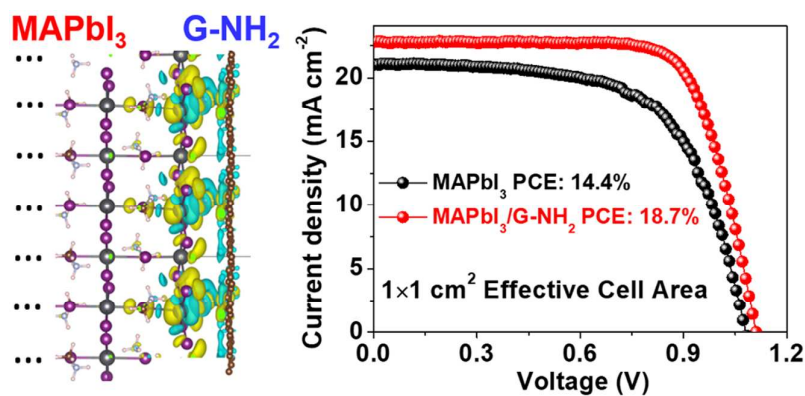
- H. Chen, F. Ye, W. Tang, J. He, M. Yin, Y. Wang, F. Xie, E. Bi, X. Yang, M. Grätzel and L. Han, *Nature*, 2017, **550**, 92-95.
- Z. Xiao, Y. Yuan, Q. Wang, Y. Shao, Y. Bai, Y. Deng, Q. Dong, M. Hu, C. Bi and J. Huang, *Mater. Sci. Eng., R*, 2016, **101**, 1-38.
- A. Mei, X. Li, L. Liu, Z. Ku, T. Liu, Y. Rong, M. Xu, M. Hu, J. Chen, Y. Yang, M. Grätzel and H. Han, *Science*, 2014, **345**, 295-298.
- NREL, <https://www.nrel.gov/pv/assets/images/efficiency-chart.png>.
- N. J. Jeon, J. H. Noh, Y. C. Kim, W. S. Yang, S. Ryu and S. I. Seok, *Nat. Mater.*, 2014, **13**, 897-903.
- Y. Zhao and K. Zhu, *J. Phys. Chem. Lett.*, 2014, **5**, 4175-4186.
- N. G. Park, M. Grätzel, T. Miyasaka, K. Zhu and K. Emery, *Nat. Energy*, 2016, **1**, 16152.

8. D. W. Dequillettes, S. M. Vorpahl, S. D. Stranks, H. Nagaoka, G. E. Eperon, M. E. Ziffer, H. J. Snaith and D. S. Ginger, *Science*, 2015, **348**, 683-686.
9. D. Y. Son, J. W. Lee, Y. J. Choi, I. H. Jang, S. Lee, P. J. Yoo, H. Shin, N. Ahn, M. Choi, D. Kim and N. G. Park, *Nat. Energy*, 2016, **1**, 16081.
10. L. Meng, J. You, T. F. Guo and Y. Yang, *Acc. Chem. Res.*, 2016, **49**, 155-165.
11. M. Liu, M. B. Johnston and H. J. Snaith, *Nature*, 2013, **501**, 395-398.
12. F. Wang, W. Geng, Y. Zhou, H. H. Fang, C. J. Tong, M. A. Loi, L. M. Liu and N. Zhao, *Adv. Mater.*, 2016, **28**, 9986-9992.
13. H. Tan, A. Jain, O. Voznyy, X. Lan, F. P. G. de Arquer, J. Z. Fan, R. Quintero-Bermudez, M. Yuan, B. Zhang, Y. Zhao, F. Fan, P. Li, L. N. Quan, Y. Zhao, Z.-H. Lu, Z. Yang, S. Hoogland and E. H. Sargent, *Science*, 2017, **355**, 722-726.
14. S. D. Stranks, G. E. Eperon, G. Grancini, C. Menelaou, M. J. Alcocer, T. Leijtens, L. M. Herz, A. Petrozza and H. J. Snaith, *Science*, 2013, **342**, 341-344.
15. G. Xing, N. Mathews, S. Sun, S. S. Lim, Y. M. Lam, M. Grätzel, S. Mhaisalkar and T. C. Sum, *Science*, 2013, **342**, 344-347.
16. C. H. Chiang and C. G. Wu, *Nat. Photonics*, 2016, **10**, 196-200.
17. L. Zuo, H. Guo, D. W. Dequillettes, S. Jariwala, N. D. Marco, S. Dong, R. Deblock, D. S. Ginger, B. Dunn, M. Wang and Y. Yang, *Sci. Adv.*, 2017, **3**, e1700106.
18. J. Xu, A. Buin, A. H. Ip, W. Li, O. Voznyy, R. Comin, M. Yuan, S. Jeon, Z. Ning, J. J. McDowell, P. Kanjanaboos, J. P. Sun, X. Lan, L. N. Quan, D. H. Kim, I. G. Hill, P. Maksymovych and E. H. Sargent, *Nat. Commun.*, 2015, **6**, 7081.
19. I. J. Park, G. Kang, M. A. Park, J. S. Kim, S. W. Seo, D. H. Kim, K. Zhu, T. Park and J. Y. Kim, *ChemSusChem*, 2017, **10**, 2660-2667.
20. M. Yang, Y. Zhou, Y. Zeng, C. S. Jiang, N. P. Padture and K. Zhu, *Adv. Mater.*, 2015, **27**, 6363-6370.
21. X. Fang, J. Ding, N. Yuan, P. Sun, M. Lv, G. Ding and C. Zhu, *Phys. Chem. Chem. Phys.*, 2017, **19**, 6057-6063.
22. C. Park, H. Ko, D. H. Sin, K. C. Song and K. Cho, *Adv. Funct. Mater.*, 2017, **27**, 1703546.
23. J. T. Wang, J. M. Ball, E. M. Barea, A. Abate, J. A. Alexander-Webber, J. Huang, M. Saliba, I. Mora-Sero, J. Bisquert, H. J. Snaith and R. J. Nicholas, *Nano Lett.*, 2014, **14**, 724-730.
24. P. You, Z. Liu, Q. Tai, S. Liu and F. Yan, *Adv. Mater.*, 2015, **27**, 3632-3638.
25. Z. Liu, P. You, C. Xie, G. Tang and F. Yan, *Nano Energy*, 2016, **28**, 151-157.
26. J. H. Im, I. H. Jang, N. Pellet, M. Gratzel and N. G. Park, *Nat Nanotechnol*, 2014, **9**, 927-932.
27. Y. Rong, Z. Tang, Y. Zhao, X. Zhong, S. Venkatesan, H. Graham, M. Patton, Y. Jing, A. M. Guloy and Y. Yao, *Nanoscale*, 2015, **7**, 10595-10599.
28. Y. Zhou, O. S. Game, S. Pang and N. P. Padture, *J. Phys. Chem. Lett.*, 2015, **6**, 4827-4839.
29. F. Ji, S. Pang, L. Zhang, Y. Zong, G. Cui, N. P. Padture and Y. Zhou, *ACS Energ. Lett.*, 2017, **2**, 2727-2733.
30. M. Hadadian, J. P. Correa-Baena, E. K. Goharshadi, A. Ummadisingu, J. Y. Seo, J. Luo, S. Gholipour, S. M. Zakeeruddin, M. Saliba, A. Abate, M. Gratzel and A. Hagfeldt, *Adv. Mater.*, 2016, **28**, 8681-8686.
31. N. Arora, M. I. Dar, A. Hinderhofer, N. Pellet, F. Schreiber, S. M. Zakeeruddin and M. Grätzel, *Science*, 2017, **358**, 768.
32. S. Song, G. Kang, L. Pyeon, C. Lim, G.-Y. Lee, T. Park and J. Choi, *ACS Energ. Lett.*, 2017, **2**, 2667-2673.
33. W. Chen, F.-Z. Liu, X.-Y. Feng, A. B. Djurišić, W. K. Chan and Z.-B. He, *Adv. Energ. Mater.*, 2017, **7**, 1700722.
34. Y. Zhou, A. L. Vasiliev, W. Wu, M. Yang, S. Pang, K. Zhu and N. P. Padture, *J. Phys. Chem. Lett.*, 2015, **6**, 2292-2297.
35. H.-C. Liao, P. Guo, C.-P. Hsu, M. Lin, B. Wang, L. Zeng, W. Huang, C. M. M. Soe, W.-F. Su, M. J. Bedzyk, M. R. Wasielewski, A. Facchetti, R. P. H. Chang, M. G. Kanatzidis and T. J. Marks, *Adv. Energ. Mater.*, 2017, **7**, 1601660.
36. M. Stollerfoht, C. M. Wolff, Y. Amir, A. Paulke, L. PerdígónToro, P. Caprioglio and D. Neher, *Energy Environ. Sci.*, 2017, **10**, 1530-1539.
37. A. Pockett, G. E. Eperon, T. Peltola, H. J. Snaith, A. Walker, L. M. Peter and P. J. Cameron, *J. Phys. Chem. C*, 2015, **119**, 3456-3465.
38. R. Long, J. Liu and O. V. Prezhdo, *J. Am. Chem. Soc.*, 2016, **138**, 3884-3890.
39. D. Zhao, M. Sexton, H. Y. Park, G. Baure, J. C. Nino and F. So, *Adv. Energ. Mater.*, 2015, **5**, 1401855.
40. J. S. Yeo, R. Kang, S. Lee, Y. J. Jeon, N. Myoung, C. L. Lee, D. Y. Kim, J. M. Yun, Y. H. Seo, S. S. Kim and S. I. Na, *Nano Energy*, 2015, **12**, 96-104.

Table of contents entry (TOC) for the manuscript:

Integration of Functionalized Graphene Nano-Network into Planar Perovskite Absorber for High Efficiency Large Area Solar Cells

Yong Wang,^a Yuanyuan Zhou,^b Taiyang Zhang,^a Ming-Gang Ju,^c Lin Zhang,^b Miao Kan,^a Yihui Li,^a Xiao Cheng Zeng,^c Nitin. P. Padture^b and Yixin Zhao^{a*}



The concept of introducing a charge-collection nano-network into perovskite layer points to a new direction towards up-scaling of high-efficiency PSCs.